Journal of Sound and Vibration 602 (2025) 118970

Contents lists available at ScienceDirect

Journal of Sound and Vibration

journal homepage: www.elsevier.com/locate/jsvi

Acoustic leak localisation based on multipath identification

Ndubuisi Uchendu *, Jennifer M. Muggleton, Paul R. White

Institute of Sound and Vibration Research (ISVR), University of Southampton, Southampton, SO17 1BJ, United Kingdom

ARTICLE INFO

Keywords:
Leakage
Acoustic
Localisation
Multipath identification
Autocorrelation
Cepstrum

ABSTRACT

This paper proposes a method for estimating wave speed and locating leaks in water pipes using multipath identification techniques. The wave speed and leak location are determined simultaneously from the relative arrival times of reflections in acoustic leak signals. Two multipath identification techniques based on the autocorrelation function and power cepstrum are derived and analysed for identifying reflections. Results show that the power cepstral technique is more robust and accurate than the autocorrelation technique. Analysis of simulation and experimental data acquired on a leakage test rig demonstrates that the proposed method is effective for locating leaks, outperforming the commonly used cross-correlation method in some cases. A practical advantage of the proposed method is capability to locate leaks without a priori knowledge of the wave speed.

1. Introduction

Timely and effective leak detection is an important task in the water industry considering the possibly disastrous consequences of water leakages. The presence of leaks undermines the safety of the water distribution networks, since leak areas can serve as entry points for contaminants, especially in low-pressure areas. Water leakages lead to increased financial loss for water companies and may result in increased costs to the consumers. They may also lead to inability to meet water demands. It is estimated that global leakage rate constitutes about 30%–50% [1]. With dwindling global freshwater supply and ever-rising demand for water driven by increasing world population, such high prevalence of water leakages represents a serious sustainability issue [2].

Acoustic methods are the primary methods for detecting and locating leaks in water distribution networks [3]. In these methods, leaks in a pipe are detected and located by analysing low-frequency acoustic signals measured on the pipe using acoustic/vibration sensors, typically hydrophones and accelerometers [4]. The most widely used acoustic technique is the cross-correlation method, in which the leak location is determined from the time delay between two signals measured on either side of the leak [5]. Referring to the typical measurement setup for this method shown in Fig. 1, the distance d_1 between the leak and the first measurement point is given by the formula

$$d_1 = \frac{d - c \cdot \tau_{\text{peak}}}{2} \tag{1}$$

where c is the acoustic wave speed in the pipe, d is the distance between the measurement points, and τ_{peak} is the time delay between the signals.

Accurate leak localisation using the cross-correlation method requires both accurate determination of the time delay and knowledge of the wave speed. Two methods commonly employed for estimating time delays between acoustic leak signals are generalised cross-correlation (GCC) and generalised phase spectrum (GPS) [6]. The GCC method determines the time delay as the

* Corresponding author.
E-mail addresses: n.uchendu@soton.ac.uk (N. Uchendu), jmm@isvr.soton.ac.uk (J.M. Muggleton), P.R.White@soton.ac.uk (P.R. White).

https://doi.org/10.1016/j.jsv.2025.118970
Received 25 March 2024; Received in revised form 11 December 2024; Accepted 15 January 2025
Available online 20 January 2025

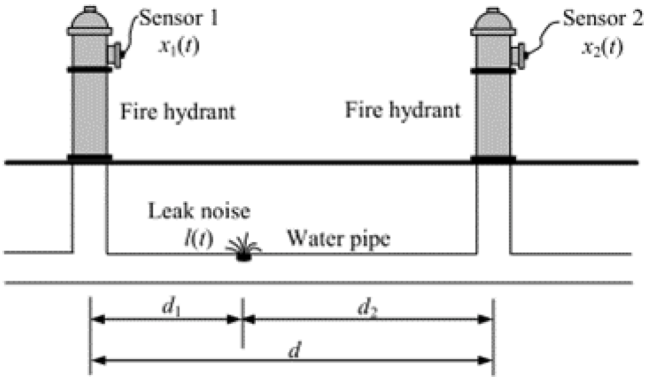

Fig. 1. Typical measurement setup for the acoustic cross-correlation method [5].

lag that maximises weighted cross-correlation function (CCF) of the signals [7], whereas the GPS method utilises weighted linear regression on the phase of the cross-power spectrum [8]. These time delay estimation (TDE) methods have been shown to be effective in various practical situations [9].

In leak detection systems, the wave speed is typically calculated using formulae that incorporate the geometric and material properties of the pipe, such as this one given in [10]:

$$c = c_{\mathrm{f}} \left(1 + \frac{B_{\mathrm{f}} D_{\mathrm{p}}}{E_{\mathrm{p}} h_{\mathrm{p}}}\right)^{-1/2} \tag{2}$$

where D_{p} is pipe diameter, h_{p} is pipe-wall thickness, E_{p} is Young's modulus of the pipe material, B_{f} is fluid bulk modulus, and c_{f} is free-field fluid wave speed. However, using the calculated wave speed can lead to a large error in the leak location estimate. This is because the actual wave speed can differ substantially from the calculated value due to changes in pipe properties over time, environmental conditions, and seasonal variations. For instance, in a series of experiments reported in [11], the measured wave speed in a buried medium density polyethylene (MDPE) pipe test rig ranged from 257 m/s to 459 m/s over a couple of months.

Uncertainties in the wave speed value present a significant challenge for leak localisation in water pipes. To address this issue, several methods have been proposed for measuring wave speed on-site concurrently with leak signal acquisition. Examples include correlation envelope method [12], hydrant simulation method [13], and cepstral matching method [14]. In the correlation envelope method, wave speed is estimated from the pipe's responses to random noise excitation at the measurement points. The hydrant simulation method determines wave speed from transient signals measured at known locations when water is released from a hydrant connected to the pipe. The cepstral matching method adjusts the wave speed until features in the cepstra of pressure transient signals acquired on either side of a fixed point on the pipe match. However, the applicability of these in-situ methods is limited by the need for extra instrumentation (such as a shaker), lack of conveniently located access points, and safety concerns related to potential damaging effects of transients. Moreover, the measured wave speed value can be significantly influenced by the properties of the excitation signal [12]. These issues highlight the need for methods that do not require a priori knowledge of wave speed for effective leak localisation. This paper develops such a method by exploiting the presence of discontinuities — features with impedance changes, such as pipe junctions, changes in cross-section, dead ends — in a pipe system.

Acoustic leak signals measured on pipe systems usually contain reflected waves due to discontinuities. In existing acoustic leak detection studies [11,15,16], these reflections are generally treated as undesirable interferences that distort TDE results and lead to inaccurate leak localisation. However, reflections provide valuable information that can be harnessed to detect and locate leaks, as demonstrated in fluid transient-based methods described in [17,18]. These methods rely on the principle that a transient wave propagating through the pipeline reflects off structural discontinuities in the pipeline. By analysing the time of flight and characteristics (energy, phase) of these reflections, the location and severity of faults, such as leaks and partial blockages, can be determined even in complex pipe networks using a single measurement. This paper employs the same principle of wave reflection to address the issue of uncertain wave speed in acoustic leak localisation.

A novel method is proposed for simultaneous estimation of wave speed and leak location through multipath identification, which involves determining the relative arrival times of the first reflections in acoustic leak signals. By identifying relative arrival times of direct-path and reflected waves in the measured leak signals, this method circumvents the need to introduce an external excitation signal (as in transient-based methods) and the requirement for pre-determined wave speed values (as in existing acoustic methods). The proposed method assumes that the acoustic waves originating from a leak in the pipe propagate predominantly as non-dispersive longitudinal waves, as supported by existing studies. To facilitate determination of arrival times of reflections, two multipath identification techniques that rely on auto-correlation function (ACF) and power cepstrum are derived and investigated for acoustic leak signals.

This work contributes to advancements in acoustic leak localisation in water distribution networks by demonstrating the viability of leveraging reflected signals for accurate wave speed estimation and leak localisation. The proposed methodology is validated through simulations and experiments to highlight its applicability to real-world networks. By leveraging reflected wave components,

the proposed method offers a complementary perspective to methods that rely only on direct-path signals, such as the graph-based method developed in [19]. This graph-based approach utilises multiple time delays between direct-path signals in a complex pipe network, represented as a graph, to localise and pinpoint leaks under a maximum likelihood estimation framework. In contrast, traditional cross-correlation method typically utilises a single time delay estimate to locate leaks, and thus may be less effective in complex networks where multiple acoustic paths exist. This study extends localisation capabilities by integrating both direct-path and reflected wave components, enhancing accuracy in networks with discontinuities and allowing for estimation of the wave speed.

This paper is organised as follows. Section 2 describes the leak localisation approach based on multipath identification. Estimation errors and resolution of potential ambiguity in the results are also discussed in this section. Section 3 explores autocorrelation and cepstral techniques for identifying reflections in acoustic leak signals. The results obtained using simulated and experimental signals are presented and discussed in Section 4. The conclusions are outlined in Section 5.

2. Multipath identification leak localisation method

The behaviour of acoustic waves in a bounded medium such as a pipe is characterised by two-dimensional modal patterns comprising circumferential modes of orders $n = 0, 1, 2, \ldots$ and the associated axial modes (denoted as s) [20]. Each circumferential mode has a cut-off frequency above which it can propagate [21]. Acoustic leak detection is most successfully executed on low-frequency signals, suggesting that these frequencies are both excited by the leak and propagate most effectively [22]. Experimental studies confirm that most leak noise energy in plastic pipes is concentrated at frequencies below 200 Hz [11,13]. At these low frequencies, a predominantly fluid-borne axisymmetric wave (denoted as $s = 1$) is responsible for transmitting most of leak signal energy in plastic pipes [10,23]. This wave corresponds to the non-dispersive fundamental circumferential mode $n = 0$, where the pipe cross-section remains circular [24]. The cut-off frequencies of higher-order modes exceed the dominant frequency range of typical leak signals [5]. Furthermore, higher-order waves exhibit significantly higher attenuation and are unlikely to propagate far enough to influence acoustic leak signal measurements [25]. Hence, waves generated by a leak in a pipe propagate primarily as longitudinal waves constrained by the pipe wall. As these waves propagate along the pipe axis, they interact with discontinuities such as joints and fittings, resulting in partial reflection of the waves. Due to the low-frequency nature of leak signals, the likelihood of exciting higher-order waves via mode conversion at discontinuities is negligible. Acoustic wave propagation in plastic pipes involves strong coupling between the pipe, the fluid, and the surrounding medium [22,26], so it can be assumed the pipe-fluid and pipe-soil interfaces do not introduce reflections.

The reflection of the leak noise (the signal generated at the leak location) at in-bracket and out-of-bracket discontinuities in a cross-correlation measurement setup is illustrated using a spatio-temporal plot in Fig. 2. Here, the terms *in-bracket* and *out-of-bracket* indicate features located within and outside the interval encompassed by the two sensors, respectively. When the incident wave reaches a discontinuity, a reflected wave ensues and propagates towards the sensors. Subsequent reflections occur from repeated interactions with the discontinuities. Consequently, the signals measured by the sensors are multipath (composite) signals comprising the direct-path wave — the wave travelling directly from the leak to the sensors — and reflected waves originating from these interactions [15]. The first reflected wave arriving at a sensor will be referred to as *primary reflection*, while later-arriving reflections will be termed *secondary reflections*. The discontinuity responsible for the primary reflection in a given sensor signal will be called the *primary discontinuity*. Identifying the arrival times of the primary reflections can be utilised to locate leaks as described below.

The arrival time of a reflected wave is determined by the travel path from the leak to a discontinuity and back to the sensor. As mentioned above, both the direct-path and reflected waves propagate primarily as non-dispersive longitudinal waves with constant wave speed. In this paper, the difference between the arrival times of the mth wave at the kth sensor and the nth wave at the ith sensor is denoted as $\tau_{ki}[m, n]$, referred to as the *time difference of arrival* (TDOA) between the two waves. For instance, $\tau_{21}[1, 1]$ indicates the TDOA between direct-path waves in the first and second signals, termed *reference time delay*.

If the primary discontinuity responsible for the primary reflection in the ith sensor signal, $x_i(t)$, $i = 1, 2$, is in-bracket, the TDOA $\tau_{ii}[2, 1]$ between the primary reflection and the direct-path wave in $x_i(t)$ is given by

$$\tau_{ii}[2,1] = \frac{d_{\mathrm{PR}} - d_{\mathrm{DP}}}{c} = \frac{2(l_{\mathrm{in}} - d_i)}{c} \tag{3}$$

where $d_{\mathrm{DP}} = d_i$ and $d_{\mathrm{PR}} = 2l_{\mathrm{in}} - d_i$ are the distances travelled by the direct-path wave and the primary reflection, respectively; d_i is the distance between the leak and the ith sensor; and l_{in} is the distance between the primary discontinuity and the ith sensor. For example, with regard to $x_1(t)$ in Fig. 2, $d_{\mathrm{DP}} = d_1$ and $d_{\mathrm{PR}} = 2l_1 - d_1$. Throughout this paper, subscript i will be used to refer to the signal/sensor being analysed, while subscript k ($k \neq i$) refers to the other sensor/signal. Simultaneous solution of Eq. (3) and the cross-correlation equation (Eq. (1)) provides estimates of the leak location $\hat{d}_i$ and wave speed $\hat{c}$:

$$\hat{d}_i = \frac{2l_{\mathrm{in}} \cdot \tau_{ki}[1,1] - d \cdot \tau_{ii}[2,1]}{2(\tau_{ki}[1,1] - \tau_{ii}[2,1])} \tag{4a}$$

$$\hat{c} = \frac{d - 2l_{\mathrm{in}}}{\tau_{ki}[1,1] - \tau_{ii}[2,1]}. \tag{4b}$$

For an out-of-bracket primary discontinuity located at a distance of l_{out} from the ith sensor, $\tau_{ii}[2, 1]$ is given by

$$\tau_{ii}[2,1] = \frac{2l_{\mathrm{out}}}{c}. \tag{5}$$

Rearranging this equation and substituting it in the cross-correlation equation yields leak location and wave speed estimates:

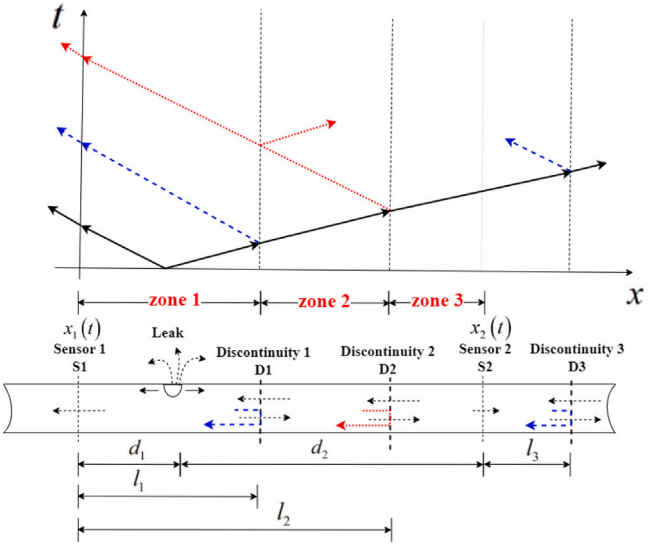

Fig. 2. Reflection of the leak noise at discontinuities. ━━ direct-path wave; - - - primary reflections; ··· secondary reflections.

$$\hat{d}_i = \frac{d \cdot \tau_{ii}[2,1] - 2l_{\text{out}} \cdot \tau_{ki}[1,1]}{2\tau_{ii}[2,1]} \tag{6a}$$

$$\hat{c} = \frac{2l_{\text{out}}}{\tau_{ii}[2,1]}. \tag{6b}$$

The distances d, l_{in}, l_{out} are known from the pipe system schematic. The reference time delay $\tau_{ki}[1,1]$ can be estimated using GCC and GPS methods [6], while the TDOA $\tau_{ii}[2,1]$ of the primary reflection can be determined using the multipath identification techniques described in the next section. Therefore, wave speed and leak location can be simultaneously estimated, as all quantities in the expressions on the right-hand side of Eqs. (4) and (6) are known or can be derived from the measured signals.

Depending on the actual locations of the leak and the discontinuities in the pipe system, the primary discontinuity can be in-bracket or out-of-bracket. According to Eq. (6), one sensor is sufficient to estimate the wave speed when the primary discontinuity is out-of-bracket. Determining the leak location using either Eq. (4a) or Eq. (6a) requires the reference time delay $\tau_{ki}[1,1]$, so the proposed method always involves two sensors bracketing the leak. This method can be viewed as *expanded* cross-correlation, in which additional information from reflections in the leak signals is harnessed to estimate the wave speed.

Accurate estimation of the wave speed and leak location using Eqs. (4) and (6) requires correct identification of the primary discontinuity. Estimation errors resulting from using the wrong discontinuity are discussed in Section 2.1. Identifying the primary discontinuity may be difficult when both in-bracket and out-of-bracket discontinuities are present in the pipe system. Hence, it is suggested to calculate the wave speed and leak location using each discontinuity. As will be illustrated later in the paper, some discontinuities will yield clearly impossible estimates (for example, negative values). Multiple discontinuities may produce *plausible* estimates (this will be defined in Section 2.2), leading to ambiguous results. Resolution of this ambiguity is discussed in Section 2.2.

2.1. Leak localisation and wave speed estimation errors

Suppose $\tilde{d}_p$ and $\tilde{c}_p$ are the leak location and wave speed estimates obtained using the *primary* discontinuity located at a distance of l_p from the sensor, i.e., values obtained by evaluating Eq. (4) with $l_{\text{in}} = l_p$ or Eq. (6) with $l_{\text{out}} = l_p$. Let the leak location and wave speed estimates obtained using a discontinuity located at a distance of l_j from the sensor be $\tilde{d}_j$ and $\tilde{c}_j$, respectively. Table 1 summarises the errors in these estimates, $\Delta d = \tilde{d}_j - \tilde{d}_p$ and $\Delta c = \tilde{c}_j - \tilde{c}_p$. The estimation errors are proportional to the distance between the chosen discontinuity and the primary discontinuity; thus, using a discontinuity located farther away from the primary discontinuity will lead to greater wave speed estimation and leak localisation errors. Correct identification of the primary discontinuity is, therefore, important. Estimates may become ambiguous when discontinuities are located close to the primary discontinuity, as discussed in the next subsection.

2.2. Ambiguity in wave speed and leak location estimates

To describe the situations under which ambiguity arises in wave speed estimation and leak localisation results, the concept of *plausibility* is introduced. Assuming there are J in-bracket discontinuities located at distances of $l_1 < l_2 < \cdots < l_J$ from the ith sensor, these discontinuities divide the pipe into $J+1$ zones: $(l_0, l_1], (l_1, l_2], \ldots, (l_J, l_{J+1}]$, where $l_0 = 0$ and $l_{J+1} = d$. Zone j encompasses the interval between l_{j-1} and l_j. If the leak is located in zone j, then the primary reflection in the sensor signal will originate from

Table 1
Leak localisation and wave speed estimation errors. $R_\tau = \frac{\tau_{ii}[2,1]}{\tau_{ki}[1,1]}$. $\Delta\tau = \tau_{ki}[1,1] - \tau_{ii}[2,1]$.

Case	Expressions for errors $\Delta d = \tilde{d}_j - \tilde{d}_p$ and $\Delta c = \tilde{c}_j - \tilde{c}_p$
Both in-bracket	$\Delta d = (l_j - l_p) \cdot (1 - R_\tau)^{-1}$ $\Delta c = \frac{2(l_p - l_j)}{\Delta\tau}$
l_p in-bracket and l_j out-of-bracket	$\Delta d = (1 - R_\tau)^{-1} \left(l_j - l_p - \frac{l_j}{R_\tau} + \frac{d}{2} \right)$ $\Delta c = \frac{2}{\Delta\tau} \left(l_p - l_j - \frac{l_j}{R_\tau} - \frac{d}{2} \right)$
l_p out-of-bracket and l_j in-bracket	$\Delta d = (1 - R_\tau)^{-1} \left(l_j - l_p + \frac{l_p}{R_\tau} - \frac{d}{2} \right)$ $\Delta c = \frac{2}{\Delta\tau} \left(l_p - l_j - \frac{l_p}{R_\tau} + \frac{d}{2} \right)$
Both out-of-bracket	$\Delta d = \frac{l_p - l_j}{R_\tau}$ $\Delta c = \frac{2(l_j - l_p)}{\tau_{ii}[2,1]}$

the jth in-bracket discontinuity at distance l_j from the sensor. For example, in Fig. 2, the primary reflection in the first signal will come from Discontinuity 1 if the leak is in zone 1, and from Discontinuity 2 if the leak is in zone 2. The leak location estimate $\tilde{d}_j$ is considered *plausible* if it falls within zone j (i.e., $l_{j-1} < \tilde{d}_j < l_j$), while the wave speed estimate $\tilde{c}_j$ is *plausible* if it satisfies $c_{\min} < \tilde{c}_j < c_{\max}$ for some threshold values $c_{\min}$ and $c_{\max}$. Estimates that do not satisfy these conditions are considered *implausible*. The threshold values $c_{\min}$ and $c_{\max}$ can be set based on historical wave speed data of pipes similar to the one under consideration or by adjusting the calculated wave speed within a certain tolerance. For the proposed method to provide accurate estimates, the actual wave speed must lie within the range defined by these thresholds.

The condition $c_{\min} < \tilde{c}_j < c_{\max}$ holds if

$$\begin{cases} \frac{d - c_{\max}\Delta\tau}{2} < l_j < \frac{d - c_{\min}\Delta\tau}{2}, & \text{when } \Delta\tau > 0 \\ \frac{d - c_{\min}\Delta\tau}{2} < l_j < \frac{d - c_{\max}\Delta\tau}{2}, & \text{when } \Delta\tau < 0 \end{cases} \tag{7}$$

where $\Delta\tau$ is defined in Table 1. Rearranging Eq. (4a) yields conditions for $\tilde{d}_j$ to satisfy $l_{j-1} < \hat{d}_j < l_j$:

$$\begin{cases} l_T < l_j < d/2, & \text{if } \tau_{ki}[1,1] > 0 \text{ and } \Delta\tau > 0 \\ d/2 < l_j < l_T, & \text{if } (\tau_{ki}[1,1] < 0 \text{ and } \Delta\tau > 0) \text{ or } (\tau_{ki}[1,1] > 0 \text{ and } \Delta\tau < 0) \\ l_j > \max\left\{ l_T, d/2 \right\}, & \text{if } \tau_{ki}[1,1] < 0 \text{ and } \Delta\tau < 0 \end{cases} \tag{8}$$

where $l_T = l_{j-1} + \left(\frac{d}{2} - l_{j-1} \right) R_\tau$; R_τ is defined in Table 1; and $\max\{\}$ denotes the maximum. By combining the conditions in Eqs. (7) and (8), the plausibility conditions for obtaining *plausible* leak and wave speed estimates when the leak is assumed to be in zone j are derived as

$$\begin{cases} \max\left\{ l_T, \frac{d - c_{\max}\Delta\tau}{2} \right\} < l_j < \frac{d - c_{\min}\Delta\tau}{2}, & \text{if } \tau_{ki}[1,1] > 0 \text{ and } \Delta\tau > 0 \\ \frac{d}{2} < l_j < \min\left\{ l_T, \frac{d - c_{\min}\Delta\tau}{2} \right\}, & \text{if } \tau_{ki}[1,1] < 0 \text{ and } \Delta\tau > 0 \\ \frac{d - c_{\min}\Delta\tau}{2} < l_j < \min\left\{ l_T, \frac{d - c_{\max}\Delta\tau}{2} \right\}, & \text{if } \tau_{ki}[1,1] > 0 \text{ and } \Delta\tau < 0 \\ \max\left\{ l_T, \frac{d - c_{\min}\Delta\tau}{2} \right\} < l_j < \frac{d - c_{\max}\Delta\tau}{2}, & \text{if } \tau_{ki}[1,1] < 0 \text{ and } \Delta\tau < 0 \end{cases} \tag{9}$$

where $\min\{\}$ denotes the minimum.

For out-of-bracket discontinuities, estimates are deemed *plausible* if they satisfy $0 < \tilde{d}_j < d$ and $c_{\min} < \tilde{c}_j < c_{\max}$. Rearranging Eq. (6) gives the plausibility conditions as

$$\frac{c_{\min} \cdot \tau_{ii}[2,1]}{2} < l_j < \max\left\{ \frac{d}{2}|R_\tau|, \frac{c_{\max} \cdot \tau_{ii}[2,1]}{2} \right\}. \tag{10}$$

The interval encompassing values of l_j that provide plausible estimates will be termed *plausibility interval* (PI). Note that the PI differs for each in-bracket discontinuity. The widths of the PIs depend on the wave speed threshold values; decreasing $c_{\max}$ and increasing $c_{\min}$ make PIs smaller. Wave speed estimation and leak localisation results will be unambiguous if only one in-bracket or only one out-of-bracket discontinuity satisfies the plausibility conditions in Eqs. (9) and (10) for a given sensor signal. If multiple discontinuities satisfy the plausibility conditions, identifying the correct estimates among the plausible estimates may be challenging.

Several approaches can be employed to resolve ambiguity in the results. The first approach is to move one of the measurement points while keeping the leak in-bracket, while the second approach involves use of *mobile* discontinuities—acoustic reflectors [27] that are moved along the pipe. The reflectors can be attached to tethered devices like the Sahara system (consisting of a sensor on an umbilical cable deployed within the pipe [3,28]), or free-swimming pipebots (small robots for autonomously exploring and detecting faults in water networks [29,30]). Only the estimates that correspond to the actual situation will remain consistent across different setups (i.e., different measurement points or reflector positions). A third option is to examine the sensor signals for additional evidence of reflections consistent with location of the leak in the assumed in-bracket zone. To illustrate this approach more clearly, consider the setup in Fig. 2. If the leak is located in zone 2, then in addition to the reflection from the out-of-bracket discontinuity D3, the Sensor 2 signal will also contain reflection from the in-bracket discontinuity D1. As discussed in the next section, each reflection present in a signal generates a distinct peak at the TDOA of that reflection in the signal's ACF and power cepstrum. Therefore, a peak will be present at lag $2(d_1 - l_1)/c$ in the ACF and power cepstrum of the Sensor 2 signal. Absence of such a peak suggests that the leak is *not* located in zone 2, and estimates obtained with the leak assumed to be in this zone can be disregarded. This third approach is useful, especially in situations where relocation of measurement points and deployment of acoustic reflectors are not feasible (for example, due to unavailability of sufficient access points).

The proposed leak localisation method *fails* in a situation where there is only one discontinuity, and its location is either coincident with the leak (thus producing no reflection) or exactly at the midpoint of the pipe. The latter case results in $\tau_{ii}[2,1] = \tau_{ki}[1,1]$, leading to indeterminate wave speed and leak location estimates in Eq. (4). Using a different measurement point so that the discontinuity is no longer at the midpoint of the pipe resolves this indeterminacy.

3. Multipath identification techniques

This section describes techniques for estimating relative arrival times of reflections in acoustic leak signals. A multipath (composite) leak signal $x(t)$ containing a reflection of the leak noise can be modelled as

$$x(t) = s(t) \otimes h_{\text{dir}} + s(t) \otimes h_{\text{ref}} + n(t) \tag{11}$$

where $s(t)$ is the leak noise, h_{dir} is the direct-path impulse response function (IRF), h_{ref} is the IRF accounting for the reflection, $n(t)$ is additive noise, and $\otimes$ denotes linear convolution. The Fourier transform (FT) $X(\omega) = \mathcal{F}\{x(t)\}$ of $x(t)$ is given by

$$X(\omega) = S(\omega)H_{\text{dir}}(\omega, d_i) + S(\omega)H_{\text{ref}}(\omega, d_{\text{PR}}) + N(\omega) \tag{12}$$

where $\mathcal{F}\{\cdot\}$ denotes FT, ω is radial frequency, $S(\omega) = \mathcal{F}\{s(t)\}$, $N(\omega) = \mathcal{F}\{n(t)\}$; $H_{\text{dir}}(\omega, d_i) = \mathcal{F}\{h_{\text{dir}}\}$ and $H_{\text{ref}}(\omega, d_{\text{PR}}) = \mathcal{F}\{h_{\text{ref}}\}$ are the direct-path and reflection frequency response functions (FRFs) that can be modelled as [5]

$$H_{\text{dir}}(\omega, d_i) = \Lambda(\omega)\exp(-|\omega|\beta d_i) \cdot \exp(-\mathrm{j}|\omega|d_i/c) \tag{13a}$$

$$H_{\text{ref}}(\omega, d_{\text{PR}}) = r \cdot \Lambda(\omega)\exp(-|\omega|\beta d_{\text{PR}}) \cdot \exp(-\mathrm{j}|\omega|d_{\text{PR}}/c) \tag{13b}$$

where r is reflection coefficient of the discontinuity responsible for the reflection, $\mathrm{j} = \sqrt{-1}$, $\Lambda(\omega)$ depends on the type of signal ($\Lambda(\omega) = 1$ for acoustic pressure signals and $\Lambda(\omega) = -\omega^2$ for acceleration signals), and β is attenuation factor (a measure of acoustic loss within the pipe wall) given by [26]

$$\beta = \frac{1}{c_{\text{f}}} \frac{\eta_{\text{p}} B_{\text{f}} D_{\text{p}}}{2E_{\text{p}} h_{\text{p}}} \left(1 + \frac{B_{\text{f}} D_{\text{p}}}{E_{\text{p}} h_{\text{p}}}\right)^{-1/2} \tag{14}$$

where ρ_{p} and η_{p} are density and loss factor of the pipe material, respectively.

Of interest in multipath identification is the TDOA $\tau_{\text{PR}} = (d_{\text{PR}} - d_i)/c$ of the reflection relative to the direct-path signal. This TDOA can be identified using autocorrelation and cepstral techniques described below for acoustic pressure signals. These techniques are also applicable to other signal types.

3.1. Autocorrelation technique

Reflections in a signal can be identified from its ACF, computed as the inverse Fourier transform (IFT) of the auto-power spectrum. Assuming $s(t)$ and $n(t)$ in Eq. (11) are uncorrelated, the auto-power spectrum $G_{xx}(\omega)$ of $x(t)$ is given by

$$\begin{aligned} G_{xx}(\omega) =& G_{ss}(\omega)\left\{\exp(-2|\omega|\beta d_i) + r^2\exp(-2|\omega|\beta d_{\text{PR}})\right\} + G_{nn}(\omega) \\ &+ 2rG_{ss}(\omega)\exp(-|\omega|\beta d_\Sigma)\cos(\omega\tau_{\text{PR}}) \end{aligned} \tag{15}$$

where $G_{ss}(\omega)$ and $G_{nn}(\omega)$ are the auto-power spectra of $s(t)$ and $n(t)$, respectively, and $d_\Sigma = d_{\text{PR}} + d_i$. It has been assumed that r is real and frequency-independent for simplicity. The ACF $R_{xx}(\tau) = \mathcal{F}^{-1}\{G_{xx}(\omega)\}$ of $x(t)$ is obtained as

$$\begin{aligned} R_{xx}(\tau) =& r \cdot R_{ss}(\tau - \tau_{\text{PR}}) \otimes \psi_r(\tau) + r \cdot R_{ss}(\tau + \tau_{\text{PR}}) \otimes \psi_r(\tau) \\ &+ R_{ss}(\tau) \otimes \psi_d(\tau) + R_{nn}(\tau) \end{aligned} \tag{16}$$

where $\mathcal{F}^{-1}\{\cdot\}$ denotes IFT, $R_{ss}(\tau) = \mathcal{F}^{-1}\{G_{ss}(\omega)\}$, $R_{nn}(\tau) = \mathcal{F}^{-1}\{G_{nn}(\omega)\}$, $\psi_r(\tau) = \mathcal{F}^{-1}\{\exp(-|\omega|\beta d_\Sigma)\}$, and $\psi_d(\tau) = \mathcal{F}^{-1}\{\exp(-2|\omega|\beta d_i) + r^2\exp(-2|\omega|\beta d_{\text{PR}})\}$. The peaks in the first and second terms in Eq. (16) occur at $\tau = \pm\tau_{\text{PR}}$, while the other terms achieve their peak at $\tau = 0$. Thus, the TDOA of the reflection can be estimated by locating the largest peak at non-zero lags in the ACF.

It can be shown that when multiple reflections are present in the signal, distinct peaks appear in the ACF at the TDOAs of these reflections. Peaks corresponding to secondary reflections are typically lower than the primary reflection peak due to signal attenuation with distance. However, primary and secondary reflection peaks may have comparable amplitudes in very noisy environments. A robust and efficient algorithm proposed in [31,32] allows identification of the primary reflection TDOA in such situations. This algorithm first estimates the number of multipaths in the two signals based on the peaks in their correlation functions. It then assigns ACF peaks to the multipaths and uses a cost function to identify the assignment that best matches the CCF peaks. The primary reflection TDOA relative to the direct-path signal is determined from this assignment.

It is important to note that correlation functions can exhibit oscillatory behaviour, characterised by peaks spaced at intervals of the inverse of the signal centre frequency [33]. This oscillation can make it difficult to unambiguously identify the true reflection TDOAs, especially in ACFs of narrowband signals, where adjacent peaks may have nearly equal heights. Also, reflected waves may be inverted relative to the direct-path wave, resulting in negative amplitudes for the corresponding peaks in the ACF. To suppress bandwidth effects and detect both in-phase and out-of-phase reflections, TDOAs should be extracted from the envelopes of the ACFs, computed as the amplitude of their Hilbert transforms [34,35].

3.2. Cepstral technique

Reflections in a signal can also be identified from its cepstrum, defined as IFT of the logarithm of the signal spectrum [36]. Two commonly used variants of the cepstrum are the power cepstrum derived from the auto-power spectrum and the complex cepstrum derived from the complex spectrum. While both variants are suitable for multipath identification, the power cepstrum is preferred in this work because it is simpler to compute, as it does not require phase unwrapping [34].

The auto-power spectrum in Eq. (15) can be rewritten as

$$G_{xx}(\omega) = G_I(\omega)\left\{1 + A(\omega)\cos(\omega\tau_{\mathrm{PR}})\right\} \tag{17}$$

where $G_I(\omega) = G_{ss}(\omega)\left\{\exp(-2|\omega|\beta d_i) + r^2\exp(-2|\omega|\beta d_{\mathrm{PR}})\right\} + G_{nn}(\omega)$, and $A(\omega) = 2r\dfrac{G_{ss}(\omega)}{G_I(\omega)}\exp(-|\omega|\beta d_\Sigma)$. The logarithm of $G_{xx}(\omega)$ is then given by

$$\log\{G_{xx}(\omega)\} = \log\left\{G_I(\omega)\right\} + \log\left\{1 + A(\omega)\cos(\omega\tau_{\mathrm{PR}})\right\}. \tag{18}$$

Since $|A(\omega)| \leq 1$ by the AM-GM inequality, the second term can be expanded using the logarithmic expansion $\log\{1+u\} = \sum_{k=1}^{\infty}\frac{u^k}{k}$ valid for $|u| \leq 1$ as

$$\log\left\{1 + A(\omega)\cos(\omega\tau_{\mathrm{PR}})\right\} = \sum_{k=1}^{\infty}(-1)^{k+1}M_k(\omega)\cos(k\omega\tau_{\mathrm{PR}}) \tag{19}$$

where $M_k(\omega)$ is the coefficient of $\cos(k\omega\tau_{\mathrm{PR}})$ obtained by applying the trigonometric identity [37]

$$\cos^k\theta = \begin{cases} \dfrac{1}{2^{k-1}}\displaystyle\sum_{n=0}^{k-1/2}\binom{n}{k}\cos((n-2k)\theta) & \text{for odd } k \\ \dfrac{1}{2^k}\binom{k}{k/2} + \dfrac{1}{2^{k-1}}\displaystyle\sum_{n=0}^{k-1/2}\binom{n}{k}\cos((n-2k)\theta) & \text{for even } k. \end{cases} \tag{20}$$

Values of $M_k(\omega)$ for the first few integers are

$$\begin{aligned} M_0(\omega) &= \frac{A^2(\omega)}{4} + \frac{3A^4(\omega)}{32} + \frac{5A^6(\omega)}{96} + \cdots \\ M_1(\omega) &= A(\omega) + \frac{A^3(\omega)}{4} + \frac{A^5(\omega)}{8} + \cdots \\ M_2(\omega) &= \frac{A^2(\omega)}{4} + \frac{A^4(\omega)}{8} + \frac{5A^6(\omega)}{64} + \cdots \end{aligned} \tag{21}$$

Substituting Eq. (19) into Eq. (18) and taking IFT yields the power cepstrum $\bar{x}(q) = \mathcal{F}^{-1}\left\{\log\left\{G_{xx}(\omega)\right\}\right\}$ of $x(t)$ as

$$\bar{x}(q) = R(q) + \frac{1}{2}\sum_{k=1}^{\infty}(-1)^{k+1}Q_k(q) \otimes \delta(q \pm k\tau_{\mathrm{PR}}) \tag{22}$$

where $R(q) = \mathcal{F}^{-1}\left\{\log\left\{G_I(\omega)\right\}\right\}$, $Q_k(q) = \mathcal{F}^{-1}\left\{M_k(\omega)\right\}$, and $\delta(\cdot)$ is the Dirac delta function. The argument q known as quefrency has units of time.

The second term in Eq. (22) contains a sequence of spikes with decreasing amplitudes at integer multiples of τ_{PR}. Assuming the spectra of the leak noise and the background noise are smooth (lacking in fine structure), $R(q)$ will be confined to low quefrencies [38]. Therefore, TDOA of the reflection can be determined as the quefrency of the dominant peak in the power cepstrum away from the origin. In cases where primary and secondary reflection peaks have comparable heights, Spiesberger's algorithm [31,32] can also be employed to identify the primary reflection TDOA, but with cepstral estimates used in place of ACF estimates. Reflection TDOAs should be identified from the envelopes of the cepstra for the same reasons previously mentioned for the ACFs.

The cepstral technique is capable of detecting reflections and producing accurate TDOA estimates in situations where the autocorrelation technique fails. Such situations involve signals containing tonal components, such as resonances and electrical

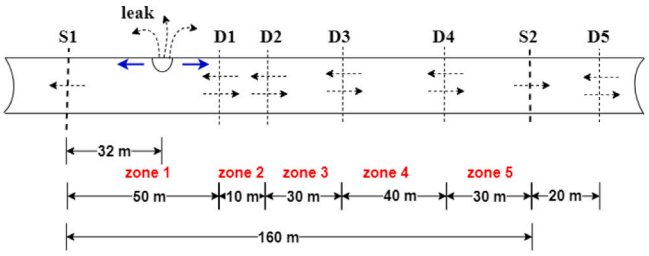

Fig. 3. Schematic of simulated pipe. S1, S2 – measurement points; D1–D5 – known discontinuities. The Figure fonts are very small overall. Please make the fonts more accessible.

mains interference [39]. Significant fluctuations contributed by the tonal components can mask reflection TDOA peaks in the ACF. Logarithmic conditioning of the auto-power spectrum mitigates the smearing effects of these fluctuations, thereby allowing for clearer detection of reflection peaks in the cepstrum. The cepstral technique is also effective in cases where the signal bandwidth is small [40] and in cases with differing transfer functions for direct-path and reflection propagation [39].

4. Results and discussion

4.1. Simulation results

The performances of multipath identification techniques and effectiveness of the proposed leak localisation method were investigated using simulated leak signals generated in a theoretical pipe, schematic of which is shown in Fig. 3. Unless otherwise specified, the pipe was assigned properties of the MDPE pipe in the leakage test rig used for experimental investigation in Section 4.2: wave speed $c = 354$ m/s and attenuation factor $\beta = 2.1 \cdot 10^{-5}$ s/m. The inter-sensor distance was set to $d = 160$ m, which is within the typical distance (90–180 m) between hydrants in the United Kingdom [41]. The discontinuities D1–D5 may represent points at which service pipes connect to the mains in a water pipe network. Each discontinuity was assigned a default reflection coefficient of 0.5.

Leak signals acquired on water pipes typically exhibit dominant low-frequency components for acoustic pressure measurements and bandpass characteristics for acceleration signals [5]. These characteristic frequency behaviours can be modelled either by assuming a flat spectrum for the signal generated at the leak location and then shaping the measured leak signals using the pipe's FRF (given in Eq. (13)), or by directly generating low-pass or bandpass signals that inherently reflect the desired frequency characteristics. The former offers greater flexibility by letting the FRF (and hence, pipe and fluid properties) determine the signal characteristics. This approach was, therefore, selected in this work to ensure that the simulated signals retain features consistent with those observed in real experimental scenarios. Acoustic leak signals at S1 and S2 were generated by filtering white Gaussian noise (denoting the leak noise) with the total FRFs between the leak location and the measurement points. Using the transmission/reflection coefficient approach described in [15], the total FRF was obtained as the sum of the direct-path and reflection path FRFs for the discontinuities. The sampling rate F_s was set to 5 kHz, and the duration of the simulated signals was 30 s.

4.1.1. Comparison of multipath identification techniques

Based on Eqs. (16) and (22), ability to detect reflections and estimate their TDOAs is affected by background noise level (quantified by signal-to-noise ratio (SNR)), pipe attenuation β, and reflection coefficient r. The effects of these factors on the performances of autocorrelation and cepstral multipath identification techniques were investigated using Monte Carlo simulations. To investigate the effects of a particular factor, its value was varied while keeping the other two constant at their default values: SNR = 0 dB, $\beta = 2.1 \cdot 10^{-5}$ s/m, $r = 0.5$. White Gaussian noise was added to the simulated leak signals to achieve the desired SNR. The test for each value of a factor consisted of 1000 Monte Carlo simulations. Different simulated leak signals and added noise were used in each run.

Two metrics were used to compare performance of autocorrelation and cepstral techniques. The first metric is the proportion of correct estimates (PCE). A TDOA estimate is considered to be correct if it is within $1/F_s = 0.2$ ms (time-domain TDOA resolution) of the true TDOA τ_{true}. This value corresponds to an absolute leak localisation error of 0.3 m in the simulated pipe. The second metric is the root-mean square error (RMSE), which is given by

$$\text{RMSE}(\tau_{\text{PR}}) = \sqrt{\frac{1}{N_s}\sum_{i=1}^{N_s}\left(\hat{\tau}_i - \tau_{\text{true}}\right)^2} \tag{23}$$

where N_s is the number of simulation runs, and τ_i is the TDOA estimate from the ith run.

Fig. 4 summarises the detection results obtained for the S1 signal. These results indicate that multipath identification becomes more challenging under higher background noise levels, lower reflection coefficients, and greater pipe attenuation, such as in large-diameter pipes [42,43]. The cepstral technique is more robust and accurate than the autocorrelation technique. Higher robustness and ability to perform well in the challenging situations mentioned in Section 3.2 make the cepstral technique the preferred choice in practical applications involving multipath identification. As already stated, its superiority is due to the logarithmic operation inherent in cepstral processing.

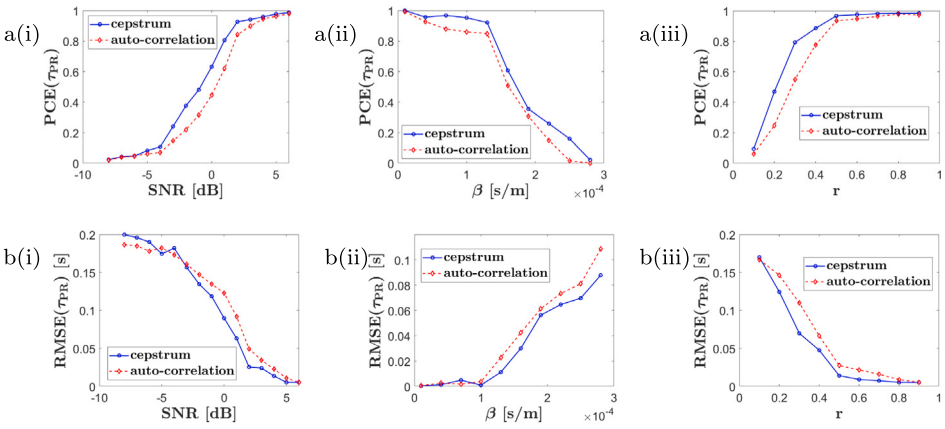

Fig. 4. Comparison of autocorrelation and power cepstral multipath identification methods. (a) PCE. (b) RMSE. Sublabels (i), (ii), (iii) indicate plots for SNR, attenuation factor, and reflection coefficient, respectively.

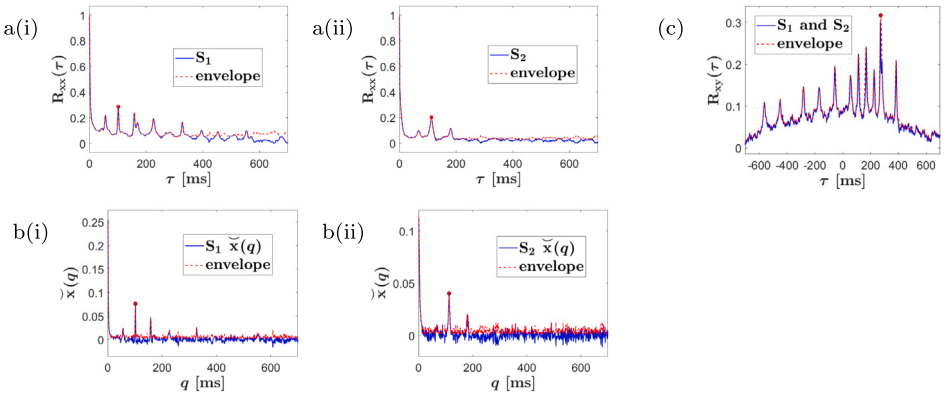

Fig. 5. Correlation functions and power cepstra of simulated leak signals with $\beta = 2, 1 \cdot 10^{-5}$ s/m, $r = 0.5$, and SNR = 3 dB. (a) ACFs. (b) Power cepstra. (c) CCF. Sublabels (i) and (ii) indicate plots for S1 and S2 signals, respectively. Red dots denote TDOA estimates.

4.1.2. Leak localisation results

The proposed method was used to locate the leak in the simulated pipe. Fig. 5 shows the correlation functions and power cepstra of the S1 and S2 signals generated with SNR, pipe attenuation, and reflection coefficient set to default values. These give the following TDOA values: $\tau_{21}[1,1] = 270.8$, $\tau_{11}[2,1] = 101.8$, and $\tau_{22}[2,1] = 113.2$ ms.

Table 2 presents the leak location and wave speed estimates obtained for each discontinuity in the pipe, along with the corresponding PIs. The wave speed thresholds were specified as $c_{\min} = 150$ and $c_{\max} = 550$ m/s. Only the discontinuities that lies within the corresponding PI — specifically, D1 for the S1 signal; D2 and D5 for the S2 signal — provide *plausible* estimates.

To resolve the ambiguity in the results obtained from the S2 signal, the first measurement point S1 was moved 5 m to the left so that $d_1 = 37$ m. Reevaluating Eqs. (4) and (6) with the new reference time delay $\tau_{21}[1,1] = 257.2$ ms gives the estimates $\hat{d}_2 = 101.6$ m and $\hat{c} = 148$ m/s for D2; and $\hat{d}_2 = 127.9$ m and $\hat{c} = 353$ m/s for D5. By comparing these values with those presented in Table 2, it can be observed that the results obtained for D5 are nearly identical in both the old and new measurement setups. In contrast, this consistency is not observed in the estimates from D2. Relocating S2, rather than S1, leads to the same observations. This indicates that the leak is *not* located in zone 2. It is, therefore, concluded that the estimates from D5 are the correct estimates.

Alternatively, additional evidence in the S1 and S2 signals can be considered as suggested in Section 2.2. If the leak is indeed located in zone 2, then the first reflections from D3 and D5 will be captured by Sensors S1 and S2, respectively. This will result in the appearance of peaks at $\frac{2 \cdot (101.1 - 100)}{156} = 15.4$ ms in the ACF and power cepstrum of the S1 signal and at $\frac{2 \cdot 20}{156} = 256.4$ ms in the ACF and power cepstrum of the S2 signal. Absence of these peaks in Figs. 5(a) to 5(e) confirms the conclusion that the leak is *not* located in zone 2. Estimates from D2 are consequently disregarded.

The leak location and wave speed estimates provided by the proposed method are close to the true value, with maximum discrepancy of 0.16 m and 0.3%, respectively. Its performance is comparable to that of the cross-correlation method, as can be observed from Table 2. It is important to note that the cross-correlation results were obtained using the true wave speed, whereas this information was not available to the proposed method. This simulation example demonstrates the viability of the method and

Table 2
Summary of simulation results. PI $l_{min} < l_j < l_{max}$ is written in the form (l_{min}, l_{max}). Yellow cells indicate *plausible* estimates.

	In-bracket discontinuity					
	Zone	$j = 1$	$j = 2$	$j = 3$	$j = 4$	$j = 5$
S1	l_j (m)	50 D1	60 D2	90 D3	130 D4	– –
	PI	(33.5, 67.3)	(61.3, 67.3)	(67.5, 67.3)	(86.2, 67.3)	
	$\hat{d}_1$ (m)	31.9	48.0	96.0	160	–
	$\hat{c}$ (m/s)	355	237	−118	−591	–
S2	l_j (m)	– –	110 D1	100 D2	70 D3	30 D4
	PI	–	(108.8, 160)	(108.8, 160)	(108.8, 160)	(108.8, 160)
	$\hat{d}_2$ (m)	–	101.2	94.1	72.9	44.7
	$\hat{c}$ (m/s)	–	156	104	−52.1	−260

	Out-of-bracket discontinuity			
S1	l_j (m)	180 D5	S2	l_j (m)	20 D5
	PI	(7.6, 30.1)		PI	(8.6, 31.4)
	$\hat{d}_1$ (m)	−399		$\hat{d}_2$ (m)	127.8
	$\hat{c}$ (m/s)	3536		$\hat{c}$ (m/s)	353

	Comparison of results				
	$\hat{c}$ (m/s)	τ_{peak} (ms)	$\hat{d}_1$ (m)	$\lvert\hat{d}_i - d_1\rvert$ (m)	$\frac{\lvert\hat{c}-c\rvert}{c}$
S1 signal	355.0	270.8	31.93	0.07	0.28%
S2 signal	353.4	−270.8	127.84	0.16	0.18%
Cross-correlation	354	270.8	32.07	0.07	0%

illustrates its capability to resolve ambiguity in the results. The method is further investigated using experimental leak signals in the next section.

4.2. Experimental results

The method presented in this paper was used to determine wave speed and locate leaks in a laboratory leakage test rig. Fig. 6(a) shows the schematic of the rig, which consists of two 6-m MDPE pipes joined with a 90° elbow. Each pipe has outer diameter of 63 mm and thickness of 6.2 mm. Leaks can be simulated by opening a valve installed on a 6-mm hole at the point marked L1, as shown in Fig. 6(b). Three 352C22 accelerometers (https://www.pcb.com/it/products-it-it?model=352c22) were mounted at the access points labelled X1, X2, and X3, as shown in Fig. 6(c). The sensitivity of the accelerometers was 1.0 mV/(ms^{-2}), and their useful frequency range was 0.3 Hz–20 kHz.

Young's modulus and loss factor of the MDPE pipes were determined using the impact excitation method [44], which calculates these quantities from equations relating them to the natural frequencies of a thin ring cut from the pipe. The measured values were $E_p = 1.2$ GPa and $\eta_p = 0.015$. This experimentally determined value of Young's modulus is higher than the typical values (0.35–0.896 GPa) reported in the literature and materials database [45,46]. Acoustic wave speed in the MDPE pipes was estimated by measuring the time delay between signals recorded at X2 and X3 when the elbow was excited with white random noise using a shaker. The average acoustic wave speed, computed over 5 measurements, is 354 m/s, with a standard deviation of 3.2 m/s.

Fig. 7 shows the correlation functions and power cepstra of signals measured at X1 and X3. These signals were acquired at a sampling rate of 40 kHz for 30 s in the presence of a leak at L1. The highly oscillatory nature of the ACFs, shown in Figs. 7(a) and 7(c), and resonant peaks in the power spectral densities (PSDs), shown in Fig. 7(f), indicate the presence of tonal components in the measured signals. Peaks induced by the tonal components mask those related to reflections, making it difficult to identify the reflection TDOAs. The main ACF peaks occur at lags 2.7 and 3.7 ms, which correspond to the inverse of the dominant resonant frequencies 377 and 270 Hz in the X1 and X3 signals, respectively. Cepstral analysis suppresses effects of tonal components, thereby allowing identification of the reflection TDOAs. The reference time delay and the TDOAs of the primary reflections in the X1 and X3 signals were determined as $\tau_{21}[1,1] = 14.2$, $\tau_{11}[2,1] = 1.2$, and $\tau_{22}[2,1] = 1.4$ ms from the envelopes of the CCF in Fig. 7(e) and the power cepstra in Figs. 7(b) and 7(d).

The in-bracket discontinuities, X2 and the elbow, divide the rig into three zones: zone 1 (between X1 and the elbow), zone 2 (between the elbow and X2), and zone 3 (between X2 and X3). Table 3 presents the results obtained for the experimental signals. Only the out-of-bracket discontinuities closest to X1 (inlet valve) and X3 (end cap 2) satisfy the plausibility conditions. These out-of-bracket discontinuities provide estimates that are close to the true values, and there is no ambiguity in the results for each signal. The reflection coefficients of the discontinuities were determined as 0.35 and 0.45 as the ratios of the amplitudes of reflected and

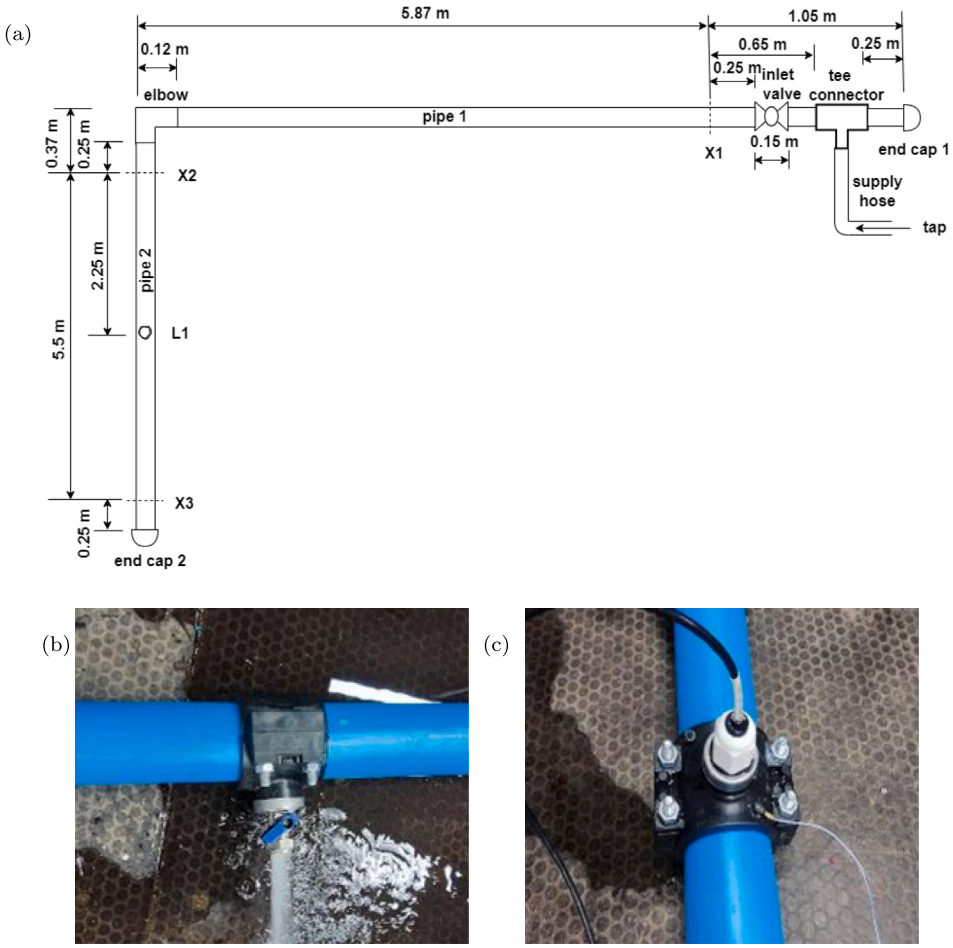

Fig. 6. Laboratory pipe leakage rig. (a) Schematic of the leakage rig; (b) Setup for leak simulation; (c) Access point for sensor installation.

incident pulses captured by sensors placed very close (<1 cm) from the discontinuities. The pulse was generated using a shaker. An alternative approach for estimating the reflection coefficient of a component is to compare the amplitudes of the power cepstral peaks corresponding to the direct-path and the primary reflection from the component, as described in [38]. This approach is useful when the components are located in an inaccessible location. Based on the peaks in the power cepstra in Figs. 7(b) and 7(d), the reflection coefficients of the inlet valve and end cap 2 are approximately 0.3 and 0.4, respectively, which are close to the experimentally determined values.

The leak location estimates were compared to those obtained using the cross-correlation method. As can be observed from Table 3, accuracy of the cross-correlation method depends on the wave speed value used. Using the wave speed $c = 279$ m/s (calculated using a typical Young's modulus value $E_p = 0.8$ GPa in Eq. (2)) results in a leak localisation error of 0.64 m, compared to just 0.11 m when the measured value is used. Typical Young's modulus values are often used to calculate the wave speed when the pipe material properties are not precisely known. The maximum error in the leak location estimates provided by the proposed method is 0.11 m. Hence, the proposed method outperforms the cross-correlation method if the latter uses the calculated wave speed.

4.3. Discussion

The numerical simulation and experimental results reported above demonstrate that the proposed method is effective for estimating wave speed and locating leaks in water pipes. Ability to accurately locate leaks without a priori knowledge of the wave speed is a major advantage of the proposed method over existing methods. This makes it particularly useful in situations where the pipe properties are uncertain and/or wave speed cannot be measured reliably on-site, such as in old and inaccessible pipes. Since the method is implemented using simple cross-correlation setup without need for extra instrumentation, it is more practically convenient and less time consuming for determining the wave speed than in-situ wave measurement methods. Owing to these advantages, the

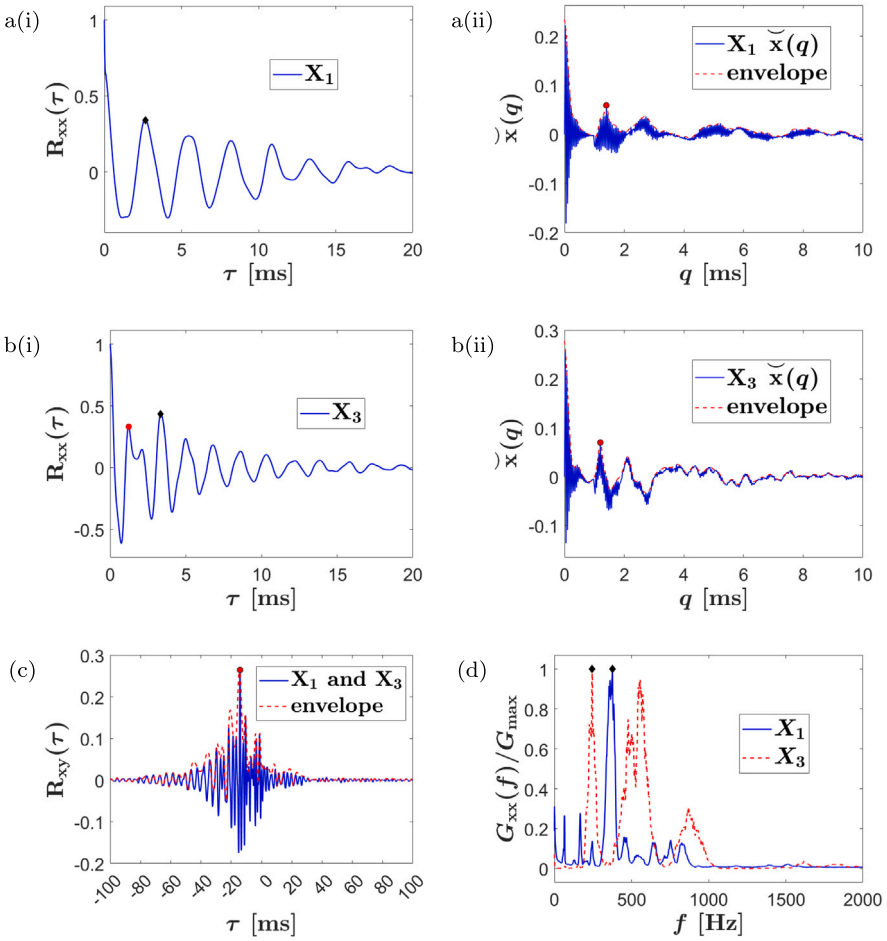

Fig. 7. Experimental leak signals measured on the leakage test rig. (a) ACF. (b) Power cepstrum. (c) CCF. (d) PSDs (normalised by their maximum values). Red dots indicate TDOA estimates. Black diamond markers indicate main resonant frequencies and resonance-induced ACF peaks.. (For interpretation of the references to colour in this figure legend, the reader is referred to the web version of this article.)

proposed method offers an attractive option for acoustic leak localisation in water distribution networks.

However, some limitations of the method can be highlighted. Like other reflectometry-based methods, the proposed method is only effective when the reflections in the measured signals can be reliably detected. As shown by the simulation results, high background noise and pipe attenuation make multipath identification more difficult. As a result, effectiveness of the method will be reduced in very noisy environments and in pipes characterised by high attenuation. Effective use of the method requires knowledge of the discontinuities in the pipe system. The presence of unknown discontinuities other than the leak may lead to inaccurate results; for example, if an unknown discontinuity is responsible for the primary reflection. Another issue is the possible ambiguity in wave speed estimation and leak localisation results. The application of the measures proposed to resolve ambiguous results may not be feasible due to practical constraints. Additionally, the wave speed thresholds used to define plausibility conditions are arbitrary and may not encompass the actual wave speed.

Future studies will aim to refine the method by addressing the highlighted shortcomings and carry out extensive experimental investigation in different water distribution networks.

5. Conclusions

A leak localisation method based on multipath identification in acoustic signals measured on a water pipe has been investigated. This method relies on detecting reflections of the leak noise in signals measured at two locations on the pipe. Autocorrelation and cepstral multipath identification techniques were derived and analysed, with results showing that the latter achieves a better performance than the former. Simulation and experimental results obtained on a leakage test rig demonstrate that the proposed method is effective for estimating wave speed and determining leak location. The proposed method achieved a maximum leak localisation error about 6 times lower than that of the conventional cross-conventional method. An important practical benefit of the method is ability to locate leaks without a priori knowledge of the wave speed.

Table 3
Summary of experimental results. Yellow cells indicate *plausible* estimates. PI $l_{\min} < l_j < l_{\max}$ is written in the form $(l_{\min}, l_{\max})$.

		In-bracket discontinuity		
	Zone	$j = 1$	$j = 2$	$j = 3$
X1	l_j (m)	5.99	6.24	11.74
		Elbow	X2	X3
	PI	(7.43,9.77)	(7.43,9.77)	(7.43,9.77)
	$\hat{d}_1$ (m)	5.98	6.21	11.21
	$\hat{c}$ (m/s)	15.4	47.4	753
X3	l_j (m)	11.74	5.75	5.5
		X1	Elbow	X2
	PI	(11.20,4.58)	(5.53,4.58)	(2.65,4.58)
	$\hat{d}_1$ (m)	12.33	5.74	5.46
	$\hat{c}$ (m/s)	−910	18.6	57.4

	Out-of-bracket discontinuity						
	$\tau_{ii}[2,1]$ (ms)	$\tau_{ki}[1,1]$ (ms)	l_j (m)	$\hat{d}_i$ (m)	$\hat{c}$ (m/s)	$\lvert\hat{d}_i - d_i\rvert$ (m)	$\frac{\lvert\hat{c}-c\rvert}{c}$
X1	1.4	PI:	(0.14,0.35)				
		−14.2	0.25	8.41	357	0.08	0.9%
			0.65	12.46	929	3.97	162%
			1.05	16.52	1500	8.03	324%
			11.99	127	17 129	119	4738%
X3	1.3	PI:	(0.13,0.54)				
		14.2	0.25	3.14	385	0.11	8.6%
			11.99	−125	18 446	128	5111%
			12.39	−129	19 062	132	5285%
			12.79	−134	19 677	137	5458%

	Cross-correlation				
	c (m/s)	τ_{peak} (ms)	$\hat{d}_1$ (m)	$\lvert\hat{d}_i - d_1\rvert$ (m)	$\frac{\lvert\hat{c}-c\rvert}{c}$
Measured speed	354	14.2	3.36	0.11	0%
Calculated speed	279	14.2	3.89	0.64	21%

CRediT authorship contribution statement

Ndubuisi Uchendu: Writing – review & editing, Writing – original draft, Validation, Investigation, Formal analysis. **Jennifer M. Muggleton:** Conceptualization, Supervision, Project administration, Funding acquisition, Methodology, Writing – review & editing . **Paul R. White:** Methodology, Supervision, Project administration, Writing – review & editing.

Declaration of competing interest

The authors declare that they have no known competing financial interests or personal relationships that could have appeared to influence the work reported in this paper.

Acknowledgements

The authors would like to thank Centre for Doctoral Training Sustainable Infrastructure Systems (CDT-SIS) University of Southampton, United Kingdom, United Kingdom Water Industry Research (UKWIR), and Petroleum Technology Development Fund (PTDF) Nigeria for sponsoring this project.

Data availability

Data will be made available on request.

References

[1] R. Liemberger, A. Wyatt, Quantifying the global non-revenue water problem, Water Supply 19 (3) (2018) 831–837, http://dx.doi.org/10.2166/ws.2018.129.
[2] D. Rogers, Leaking water networks: An economic and environmental disaster, Procedia Eng. 70 (2014) 1421–1429, http://dx.doi.org/10.1016/j.proeng.2014.02.157.
[3] Z. Liu, Y. Kleiner, B. Rajani, L. Wang, W. Condit, Condition Assessment Technologies for Water Transmission and Distribution Systems, Vol. EPA/600/R-12/017, EPA, USA, 2012.

[4] H.V. Fuchs, R. Riehle, Ten years of experience with leak detection by acoustic signal analysis, Appl. Acoust. 33 (1) (1991) 1–19, http://dx.doi.org/10.1016/0003-682x(91)90062-j.
[5] Y. Gao, Leak Detection in Plastic Water Pipes (PhD), University of Southampton, 2006, https://eprints.soton.ac.uk/465828/.
[6] M.J. Brennan, Y. Gao, P.F. Joseph, On the relationship between time and frequency domain methods in time delay estimation for leak detection in water distribution pipes, J. Sound Vib. 304 (1–2) (2007) 213–223, http://dx.doi.org/10.1016/j.jsv.2007.02.023.
[7] C. Knapp, G. Carter, The generalized correlation method for estimation of time delay, IEEE Trans. Acoust. Speech Signal Process. 24 (4) (1976) 320–327, http://dx.doi.org/10.1109/tassp.1976.1162830.
[8] Z. Zhao, Z. Hou, The generalised phase spectrum method for time delay estimation, in: Proceedings of IEEE Conference on Acoustics, Speech, and Signal Processing, Vol. 3, 1984, pp. 1–4, http://dx.doi.org/10.1109/ICASSP.1984.1172709.
[9] Y. Gao, M.J. Brennan, P.F. Joseph, A comparison of time delay estimators for the detection of leak noise signals in plastic water distribution pipes, J. Sound Vib. 292 (3–5) (2006) 552–570, http://dx.doi.org/10.1016/j.jsv.2005.08.014.
[10] R.J. Pinnington, A.R. Briscoe, Externally applied sensor for axisymmetric waves in a fluid filled pipe, J. Sound Vib. 173 (4) (1994) 503–516, http://dx.doi.org/10.1006/jsvi.1994.1243.
[11] F.C.L. Almeida, Improved Acoustic Methods for Leak Detection in Buried Plastic Water Distribution Pipes (PhD), University of Southampton, 2013, https://eprints.soton.ac.uk/355964/.
[12] F.C.L. Almeida, M.J. Brennan, P.F. Joseph, S. Dray, S. Whitfield, A.T. Paschoalini, Towards an in-situ measurement of wave velocity in buried plastic water distribution pipes for the purposes of leak location, J. Sound Vib. 359 (2015) 40–55, http://dx.doi.org/10.1016/j.jsv.2015.06.015.
[13] O. Hunaidi, W. Chu, A. Wang, W. Guan, Detecting leaks in plastic pipes, J. Am. Water Work. Assoc. 92 (2) (2000) 82–94, http://dx.doi.org/10.1002/j.1551-8833.2000.tb08819.x.
[14] J.D. Shucksmith, J.B. Boxall, W.J. Staszewski, A. Seth, S.B.M. Beck, Onsite leak location in a pipe network by cepstrum analysis of pressure transients, J. Am. Water Work. Assoc. 104 (8) (2012) E457–E465, http://dx.doi.org/10.5942/jawwa.2012.104.0108.
[15] Y. Gao, M.J. Brennan, P.F. Joseph, On the effects of reflections on time delay estimation for leak detection in buried plastic water pipes, J. Sound Vib. 325 (3) (2009) 649–663, http://dx.doi.org/10.1016/j.jsv.2009.03.037.
[16] P.C. Ayala Castillo, An Investigation into Some Signal Processing Techniques for the Development of a Low-Cost Acoustic Correlator to Detect and Locate Leaks in Buried Water Pipes (PhD), São Paulo State University, 2019, https://repositorio.unesp.br/server/api/core/bitstreams/60873347-78fc-4899-8a09-98ea3f751172/content.
[17] B. Brunone, F. Maietta, C. Capponi, A. Keramat, S. Meniconi, A review of physical experiments for leak detection in water pipes through transient tests for addressing future research, J. Hydraul. Res. 60 (6) (2022) 894–906, http://dx.doi.org/10.1080/00221686.2022.2067086.
[18] B. Brunone, F. Maietta, C. Capponi, H.-F. Duan, S. Meniconi, Detection of partial blockages in pressurized pipes by transient tests. A review of the physical experiments, Fluids 8 (1) (2023) 19, http://dx.doi.org/10.3390/fluids8010019.
[19] P. Agrawal, S. Fong, D. Friesen, S. Narasimhan, Maximum likelihood estimation to localize leaks in water distribution networks, J. Pipeline Syst. Eng. Pr. 14 (4) (2023) 04023038, http://dx.doi.org/10.1061/JPSEA2.PSENG-1494.
[20] G. Pavic, Vibroacoustical energy flow through straight pipes, J. Sound Vib. 143 (3) (1992) 411–429, http://dx.doi.org/10.1016/0022-460X(92)90776-T.
[21] L. Cremer, M. Heckl, B. Petersson, Structure-Borne Sound: Structural Vibrations and Sound Radiation at Audio Frequencies, Springer Berlin, Heidelberg, 2010.
[22] J.M. Muggleton, M.J. Brennan, R.J. Pinnington, Wavenumber prediction of waves in buried pipes for water leak detection, J. Sound Vib. 249 (5) (2002) 939–954, http://dx.doi.org/10.1006/jsvi.2001.3881.
[23] Y. Gao, Y. Liu, Theoretical and experimental investigation into structural and fluid motions at low frequencies in water distribution pipes, Mech. Syst. Signal Process. 90 (2017) 126–140, http://dx.doi.org/10.1016/j.ymssp.2016.12.018.
[24] C.R. Fuller, F.J. Fahy, Characteristics of wave propagation and energy distributions in cylindrical elastic shells filled with fluid, J. Sound Vib. 81 (4) (1982) 501–518, http://dx.doi.org/10.1016/0022-460x(82)90293-0.
[25] E. Franco, M. Andrade, R. Higuti, J. Adamowski, F. Buiochi, Acoustic transmission with mode conversion phenomenon, ABCM Symp. Ser. Mechatron. 2 (2006) 113–120.
[26] J.M. Muggleton, M.J. Brennan, P.W. Linford, Axisymmetric wave propagation in fluid-filled pipes: wavenumber measurements in in vacuo and buried pipes, J. Sound Vib. 270 (1–2) (2004) 171–190, http://dx.doi.org/10.1016/s0022-460x(03)00489-9.
[27] O. Sawant, A. Bhowmick, T.V. Sreenivas, Enhanced directional sensitivity using acoustic dish reflector, in: 2018 International Conference on Signal Processing and Communications, SPCOM, 2018, pp. 162–166, http://dx.doi.org/10.1109/SPCOM.2018.8724424.
[28] WRC, Sahara pipeline inspection system, 2024, https://wrcgroup.com/services/sahara-pipeline-leakage-inspection.
[29] Y. Yu, K. Horoshenkov, R. Worley, S. Anderson, Robotic sensing for buried pipes with sound waves, J. Acoust. Soc. Am. 154 (A68) (2023) http://dx.doi.org/10.1121/10.0022823.
[30] J. Zhang, X. Niu, A. Croxford, B. Drinkwater, Pipe inspection using guided acoustic wave sensors integrated with mobile robots, NDT & T Int. 102929 (2023) http://dx.doi.org/10.1016/j.ndteint.2023.102929.
[31] J.L. Spiesberger, Identifying cross-correlation peaks due to multipaths with application to optimal passive localization of transient signals and tomographic mapping of the environment, J. Acoust. Soc. Am. 100 (2) (1996) 910–917, http://dx.doi.org/10.1121/1.416250.
[32] J.L. Spiesberger, Linking auto- and cross-correlation functions with correlation equations: Application to estimating the relative travel times and amplitudes of multipath, J. Acoust. Soc. Am. 104 (1) (1998) 300–312, http://dx.doi.org/10.1121/1.423257.
[33] E. Weinstein, A. Weiss, Fundamental limitations in passive time-delay estimation–Part II: Wide-band systems, IEEE Trans. Acoust. Speech Signal Process. 32 (5) (1984) 1064–1078, http://dx.doi.org/10.1109/TASSP.1984.1164429.
[34] A. Oppenheim, R. Schafer, Discrete-Time Signal Processing, third ed., Pearson, Upper Saddle River, New Jersey, 2010.
[35] L. Marple, Computing the discrete-time "analytic" signal via FFT, IEEE Trans. Signal Process. 47 (9) (1999) 2600–2603, http://dx.doi.org/10.1109/78.782222.
[36] B. Bogert, M. Healy, J. Tukey, The quefrency analysis of time series for echoes: Cepstrum, pseudo-autocovariance, cross-cepstrum and saphe-cracking, in: M. Rosenblatt (Ed.), Time Series Analysis, Wiley, New York, 1963, pp. 209–243.
[37] W.H. Beyer, CRC Standard Mathematical Tables, 28th ed., CRC Press, Boca Raton, Fla., 1987.
[38] J.S. Bolton, E. Gold, The application of cepstral techniques to the measurement of transfer functions and acoustical reflection coefficients, J. Sound Vib. 93 (2) (1984) 217–233, http://dx.doi.org/10.1016/0022-460x(84)90309-2.
[39] A. Lindgren, K. Gong, Measurement of the relative delay between signals propagating in a multipath environment, in: Proceedings of the IEEE International Conference on Engineering in the Ocean Environment, Ocean '74, 1974, pp. 293–298, http://dx.doi.org/10.1109/oceans.1974.1161438.
[40] J.C. Hassab, Underwater Signal and Data Processing, CRC Press, Boca Raton, Florida, 1989.
[41] HMFSI, Fire Service Manuals Volume 1: Fire Service Technology, Equipment and Media, Stationery Office, HM Fire Service Inspectorate, London, UK, 1998.
[42] R. Long, P. Cawley, M. Lowe, Acoustic wave propagation in buried iron water pipes, Proc.: Math. Phys. Eng. Sci. 459 (2039) (2003) 2749–2770, http://www.jstor.org/stable/3560123.
[43] O. Hunaidi, Acoustic leak detection survey strategies for water distribution pipes, Constr. Technol. Updat. 79 (2012) 1–5.

[44] J.D. Lord, R.M. Morrell, Measurement Good Practice Guide No. 98: Elastic Modulus Measurement, National Physical Laboratory, Middlesex, UK, 2006, pp. 41–65.
[45] M.F. Ashby, Appendix A - data for engineering materials, in: Materials Selection in Mechanical Design, fourth ed., Butterworth-Heinemann, Oxford, 2011, pp. 495–523, http://dx.doi.org/10.1016/B978-1-85617-663-7.00018-7.
[46] MatWeb, Overview of materials for Medium Density Polyethylene (MDPE), Molded, 2024, https://www.matweb.com/search/DataSheet.aspx?MatGUID=012541b0d0a14512ab711efc8411e61e, Online: accessed 23 September 2024.